



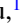


Pressure-driven change of ground state of Ce₃Pd₃Bi₄: A DFT+DMFT studyShuai-Kang Zhang ¹, Yuan-Ji Xu ², Cui-E Hu ^{3,*}, Yan Cheng ^{1,†}, Jun Zhu ¹ and Guang-Fu Ji⁴¹College of Physics, Sichuan University, Chengdu 610064, China²Institute for Applied Physics, University of Science and Technology Beijing, Beijing 100083, China³College of Physics and Electronic Engineering, Chongqing Normal University, Chongqing 400047, China⁴National Key Laboratory for Shock Wave and Detonation Physics Research, Institute of Fluid Physics, China Academy of Engineering Physics (CAEP), Mianyang 621900, China

(Received 16 June 2022; revised 10 September 2022; accepted 26 October 2022; published 9 November 2022)

A candidate material for strongly correlated topological materials, Ce₃Pd₃Bi₄ has attracted much attention, but its ground state remains controversial. Compared with the typical Kondo insulator Ce₃Pt₃Bi₄, two possibilities of ground states are proposed: Ce₃Pd₃Bi₄ is either a spin-orbit-driven topological semimetal or a Kondo insulator with less Kondo coupling strength than platinum. Here, we performed density functional theory (DFT) + dynamical mean field theory (DMFT) calculations on Ce₃Pd₃Bi₄ under different pressures to clarify its ground state, as pressure can tune the strength of Kondo coupling without affecting the strength of spin-orbit coupling. We found Ce₃Pd₃Bi₄ has a metallic ground state and becomes insulating with increasing pressure at a low temperature. And as the pressure increased to 2 GPa, a hybridization energy gap can be observed at 10 K. As the pressure increased to 5 GPa, the electronic structure of Ce₃Pd₃Bi₄ is even similar to that of the Kondo insulator Ce₃Pt₃Bi₄ under ambient pressure, and a clear hybridization energy gap (~3 meV) appears at 20 K. Our results not only demonstrate that the key factor controlling the different ground states between the two compounds is Kondo physics, rather than spin-orbit coupling, but also confirm that Ce₃Pd₃Bi₄ is an ideal material to tuning the ground states by changing the strength of hybridization by pressure.

DOI: [10.1103/PhysRevB.106.205115](https://doi.org/10.1103/PhysRevB.106.205115)**I. INTRODUCTION**

The hybridization between *f*-electrons with conduction band electrons combined with the strong Coulomb interaction between *f*-electrons in heavy-fermion systems lead to strong temperature dependence of electronic structures. Recently, heavy-fermion systems have received much attention due to the discovery of electronic band topology [1–4]. As a proximate semimetal, the ground state of non-centrosymmetric Ce₃Pd₃Bi₄ is still controversial [5]. On the one hand, some theories suggest the possible existence of Weyl Kondo semimetal (WKSM) phases in strongly correlated materials with broken inversion symmetry [4,6–9]. It is experimentally found that the contribution of electrons to specific heat is consistent with that predicted by WKSM theory [6,8]. Furthermore, this is considered a sign of the lack of a well-defined energy gap due to the weak dependence of resistance on temperature [8]. On the other hand, some experiments suggest that there is an energy gap in the ground state—for example, the measurement of resistivity and Hall resistivity. In addition, by fitting the low-temperature specific heat energy with the Schott–Schott Kondo resonance model, which has a resonance of Lorenz shape and width Δ at the Fermi energy, an energy gap (1.7 ± 0.2 meV) is obtained [10].

However, Ce₃Pt₃Bi₄, obtained by replacing palladium of the same main group with platinum, is a typical Kondo in-

ulator [5,11–14]. According to WKSM theory, the reduction of the spin-orbit coupling (SOC) caused by the replacement of platinum with palladium is the main driving factor for the disappearance of the Kondo gap in Ce₃Pd₃Bi₄ [6,8]. However, even with the similar lattice parameters, the radius of Pd-4*d* is smaller than that of Pt-5*d*, which obviously affects the strength of hybridization between them. Recently, Ajeesh *et al.* [15] applied hydrostatic pressure to Ce₃Pd₃Bi₄ to tune the strength of Kondo coupling without changing the strength of the SOC. They found that Ce₃Pd₃Bi₄ behaves like an insulator, by measuring electrical resistivity when the pressure is applied. However, how hybridization is controlled by pressure requires further theoretical investigation. Recently, Xu *et al.* [16] studied the effect of strain on Ce₃Pd₃Bi₄ using density functional theory (DFT) + dynamical mean field theory (DMFT). However, there is currently a lack of comparative studies on Ce₃Pd₃Bi₄ under pressure and Ce₃Pt₃Bi₄.

Here, we performed DFT + DMFT calculations on Ce₃Pd₃Bi₄ under different pressures to investigate its ground states and explore implicit factors. By comparing with the electronic structures of Ce₃Pt₃Bi₄, we verified that Ce₃Pd₃Bi₄ is a metallic state under ambient pressure and it becomes a Kondo insulator with under low pressure. Furthermore, we conclude that the reason for the different ground states of two compounds is not the different strength of the SOC, but the different strength of hybridization. We also deduced that Ce₃Pd₃Bi₄ is at the edge of forming coherent hybridization under ambient pressure, hence the pressure can easily tune the gap by adjusting the strength of hybridization.

* cuiehu@cqu.edu.cn

† ycheng@scu.edu.cn

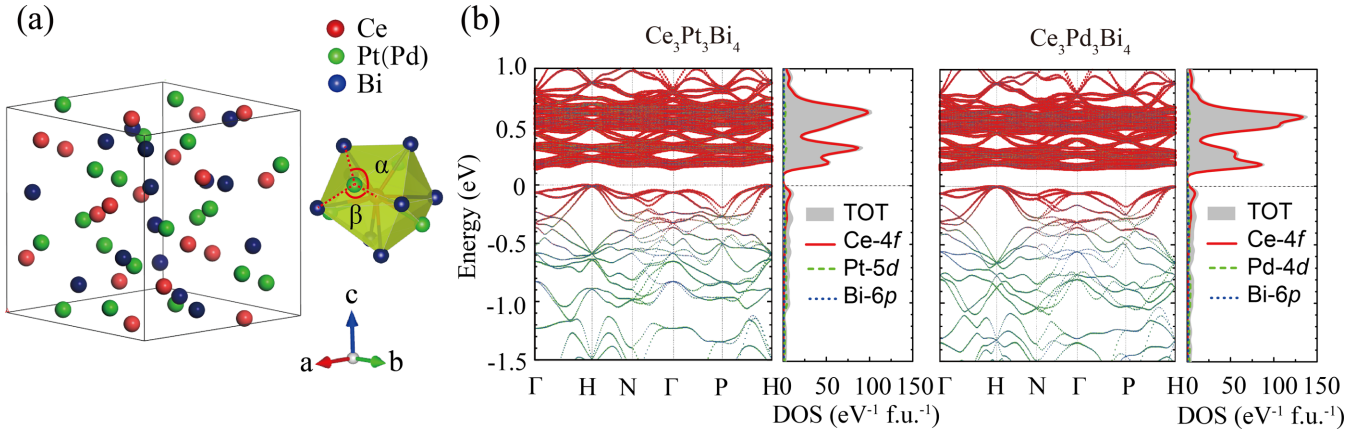


FIG. 1. The structure of $\text{Ce}_3\text{Pt}(\text{Pd})_3\text{Bi}_4$ and the electronic structure of $\text{Ce}_3\text{Pt}(\text{Pd})_3\text{Bi}_4$ from DFT with SOC. (a) The structure of $\text{Ce}_3\text{Pt}(\text{Pd})_3\text{Bi}_4$. The red, green, and blue balls represent cesium, palladium/plutonium, and bismuth atoms, respectively. (b) The band structure and DOS of $\text{Ce}_3\text{Pt}(\text{Pd})_3\text{Bi}_4$. The gray area is the total spectral density, and the red solid lines, green dashed lines, and blue dotted lines represent $\text{Ce-}4f$, $\text{Pt-}5d$ ($\text{Pd-}4d$), and $\text{Bi-}6p$, respectively.

II. COMPUTATIONAL METHODS

The DFT calculations were performed using the full-potential linearized augmented plane-wave WIEN2k code [17]. The radius of atomic spheres R multiply plane-wave cutoff K_{max} was set to 8.0 and the k -mesh was set to $12 \times 12 \times 12$. The exchange-correlation functional is the conventional Perdew–Burke–Ernzerhof functional [18]. The SOC effect was taken into account in a second-order variational manner in the WIEN2k code. The lattice parameters of $\text{Ce}_3\text{Pd}_3\text{Bi}_4$ under pressure were estimated by equation-of-state fitting, and the atomic coordinates were optimized using the WIEN2k code. The DFT + DMFT method combines realistic band-structure calculation by DFT with the nonperturbative many-body treatment of local interaction effects in DMFT [19,20]. For the fully consistent DFT + DMFT calculations, this method has been successfully applied to some strongly correlated electronic materials [21,22]. Here we perform fully charged self-consistent calculations to explore the detailed electronic structure of $\text{Ce}_3\text{Pt}_3\text{Bi}_4$ and $\text{Ce}_3\text{Pd}_3\text{Bi}_4$ using the DFT + DMFT method. The implementation of this method is divided into DFT and DMFT parts, which are solved separately using the WIEN2k code and the eDMFTF package [17,19,23]. The same RK_{max} , k -mesh, and exchange-correlation functional as the DFT calculations are used here. We also consider SOC in our calculations, and the onsite interaction parameters of $\text{Ce-}4f$, Hubbard U , and Hund exchange J are $U = 6.0$ eV and $J = 0.7$ eV, which is the conventional choice [24–26]. The $\text{Pt-}5d$ - and $\text{Pd-}4d$ -electrons are considered to be noncorrelated due to their larger bandwidth. We ignore the off-diagonal components of the hybridization function. This avoids the negative sign problem and generally does not have a serious impact on the result [23]. The continuous-time quantum Monte Carlo impurity solver [20] was employed to solve the resulting multiorbital Anderson impurity model. We made a severe truncation ($N \in [0, 1, 2, 3]$) for the local Hilbert space to reduce the computational burden. The long-range magnetic order is not considered in the DFT and DFT + DMFT calculations in this work due to the two materials having a paramagnetic ground state.

III. RESULTS AND DISCUSSION

$\text{Ce}_3\text{Pt}_3\text{Bi}_4$ and $\text{Ce}_3\text{Pd}_3\text{Bi}_4$ belong to cubic crystal system, as shown in Fig. 1(a), and the space group is $I-43d$ (No. 220). To account for the difference between their ground states [5,11,12,15], we first calculated the paramagnetic electronic structures by DFT with SOC. As shown in Fig. 1(b), there is no significant difference between the two electronic structures. The ground states are all insulators with an energy gap of about 0.15 eV, and the energy band near the Fermi energy (E_F) are mainly derived from $\text{Ce-}4f$. The density of states (DOS) of $\text{Pt-}5d$ ($\text{Pd-}4d$) is of the same order of magnitude as $\text{Bi-}6p$, which are far smaller than $\text{Ce-}4f$. The occupancy numbers of $\text{Pd-}4d$ and $\text{Pt-}5d$ are 8.2 and 7.7, respectively. Their bandwidths are too broad (-5 eV to 1 eV) and the correlation effects of $\text{Pd-}4d$ and $\text{Pt-}5d$ are much weaker than that of $\text{Ce-}4f$, so $\text{Pt-}5d$ - and $\text{Pd-}4d$ -electrons can be treated as noncorrelated electrons. The occupancy numbers of $\text{Ce-}4f$ -electrons are all about 0.98, and $\text{Ce-}4f$ peaks appear at about 0.2 eV and 0.6 eV above the E_F . This result is not surprising, since the $\text{Ce-}4f$ -electrons in the DFT calculations are treated as itinerant with a closed core treatment [5]. The static $+U$ correction moves an empty (full) f -band up (down). Hence, the DFT + U calculations for $\text{Ce-}4f$ will get a ground state with a larger gap.

To get a better treatment of $\text{Ce-}4f$ correlated electrons, we should give a better treatment of the correlation effect. We further performed the DFT + DMFT calculations on the two compounds. We first focus on $\text{Ce}_3\text{Pt}_3\text{Bi}_4$, which has been confirmed with a Kondo insulator ground state in former research [5]. Figure 2 shows the electronic structure of $\text{Ce}_3\text{Pt}_3\text{Bi}_4$ at different temperatures. The $\text{Ce-}4f_{5/2}$ and $\text{Ce-}4f_{7/2}$ bands are located near the E_F and about 0.35 eV above the E_F , respectively, as shown in Figs. 2(a) and 2(b). The system exhibits metallic properties at high temperatures. It can be clearly seen that the localized $\text{Ce-}4f$ -electrons form a blurry band near the E_F , and some conduction bands, which are mainly $\text{Pt-}5d$ and $\text{Bi-}6p$ across the E_F between Γ – H , H – N , and P – H at 300 K, as shown in Fig. 2(c). As the temperature decreases, the $\text{Ce-}4f_{5/2}$ flat bands gradually form and start to hybridize

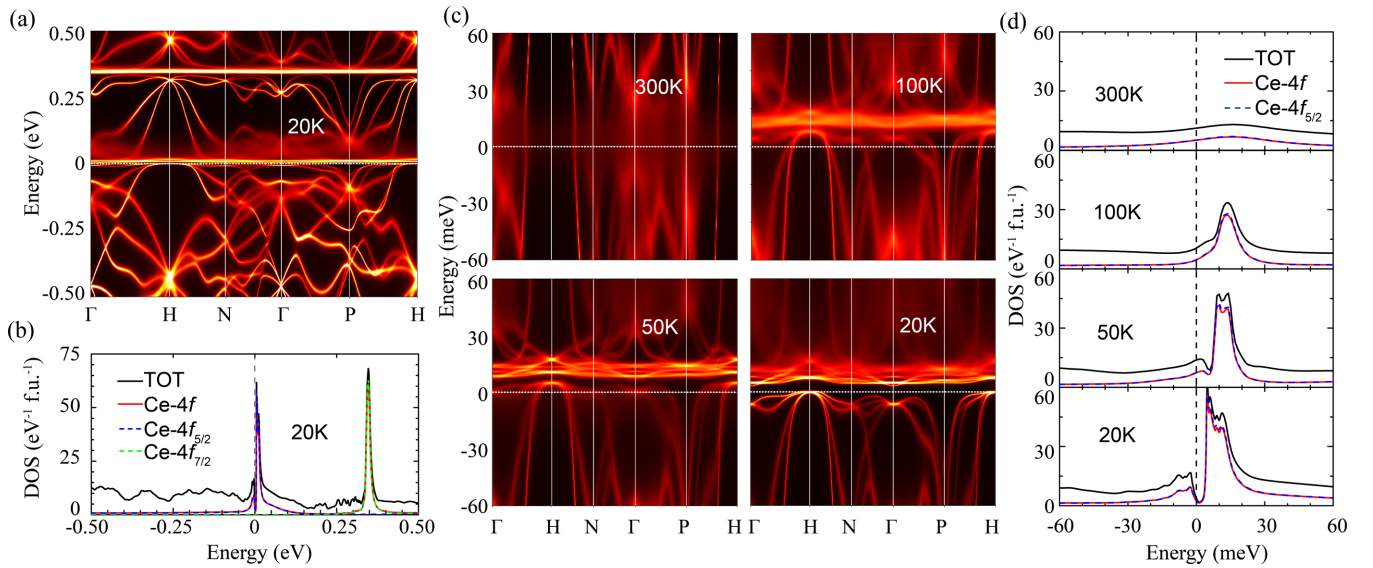


FIG. 2. The electronic structure of $\text{Ce}_3\text{Pt}_3\text{Bi}_4$ from DFT + DMFT. The momentum-resolved spectral functions (a) and spectral density (b) at 20 K. The momentum-resolved spectral functions (c) and spectral density (d) at 300, 100, 50, and 20 K. The black solid lines, red solid lines, blue dashed lines, and green dashed lines represent total spectral density, Ce-4*f*, Ce-4*f*_{5/2}, and Ce-4*f*_{7/2} contributions, respectively.

with the conduction bands. The hybridization has occurred at 100 K, but no hybridization gaps. It can be seen that a clear hybridization gap appears at 50 K in the momentum-resolved spectral functions shown in Fig. 2(c). At 50 K, 20 K, and 10 K, the occupancy numbers of Ce-4*f*_{5/2} are 1.020, 1.039, and 1.096, respectively. As the temperature decreases, the Ce-4*f* occupancy number increases and the E_F shifts upward, but the band shape does not change, as shown in Fig. 2(c). The energy gap is about 3 meV at 20 K. Experimentally, the hybridization gap starts to form below 100 K, and the maximum value is about 4.3 meV at 50 K [27–30]. Compared with DFT, the ground state obtained by DFT + DMFT is in good agreement with the experiment. For the DFT + DMFT calculations of $\text{Ce}_3\text{Pt}_3\text{Bi}_4$, the numbers of Ce-4*f* occupation are about 1.04 at all temperatures, indicating that the valence fluctuations in the system are negligible. These results are also consistent with previous theoretical calculations [5]. Therefore, $\text{Ce}_3\text{Pt}_3\text{Bi}_4$ is a typical Kondo insulator in which the Ce-4*f*_{5/2}-electrons are coupled with conduction electrons.

However, our results of DFT + DMFT show that the electronic structure of $\text{Ce}_3\text{Pd}_3\text{Bi}_4$ is very different from that of $\text{Ce}_3\text{Pt}_3\text{Bi}_4$, although $\text{Ce}_3\text{Pd}_3\text{Bi}_4$ has almost the same lattice parameters and slightly different bismuth atomic coordinates compared with $\text{Ce}_3\text{Pt}_3\text{Bi}_4$. As shown in Figs. 3(a) and 3(b), like $\text{Ce}_3\text{Pt}_3\text{Bi}_4$, the Ce-4*f*_{5/2} and Ce-4*f*_{7/2} flat bands appear near the E_F and at 0.35 eV above the E_F , respectively. The localized 4*f* flat bands hybridize with the conduction band at a low temperature. However, a clear hybridization gap cannot be found in the spectral function, even if the temperature is lowered to 10 K [Figs. 3(d) and 3(e)]. Although we did not perform DFT + DMFT calculations at lower temperatures, previous theoretical calculations by Cao *et al.* [5] showed that there is still no apparent hybridization gap even when the temperature is lowered to 4 K. One possible reason for the different electronic structures is the stronger strength of the SOC of platinum than that of palladium. However, there is no obvious difference of SOC splitting near the E_F between

two compounds [5]. The other possible reason is the different strengths of Kondo coupling in $\text{Ce}_3\text{Pt}_3\text{Bi}_4$ and $\text{Ce}_3\text{Pd}_3\text{Bi}_4$. Applying pressure is a clean way to tune the strength of coupling without breaking symmetry or changing the strength of SOC.

Therefore, we can verify this conjecture by calculating the electronic structure of $\text{Ce}_3\text{Pd}_3\text{Bi}_4$ under different pressures. Due to the lack of experimental lattice parameters data under different pressures, we first calculate the ground-state energy under different lattice parameters, and the lattice parameters under different pressure estimated by equation-of-state fitting using the WIEN2k code. Finally, the atomic coordinates are optimized using the WIEN2k code. In Table I, we list the crystal structure information of $\text{Ce}_3\text{Pt}_3\text{Bi}_4$ and $\text{Ce}_3\text{Pd}_3\text{Bi}_4$ at different pressures. Compared with DFT + *U*, the lattice constant obtained by DFT is closer to the experiment. However, DFT + *U* can result in a relatively small lattice constant, which is the same as that in some other material calculations [31,32]. Therefore, we use the structure obtained by the DFT method in this work. Although the lattice parameter of $\text{Ce}_3\text{Pd}_3\text{Bi}_4$ is slightly smaller than that of $\text{Ce}_3\text{Pt}_3\text{Bi}_4$ under ambient pressure, the radius of Pd-4*d* is smaller than that of Pt-5*d*, hence the hybridization strength of $\text{Ce}_3\text{Pd}_3\text{Bi}_4$ may be smaller.

As shown in Fig. 1(a), cesium atoms are surrounded by Pt(Pd) and bismuth atoms, and there are two different Pd(Pt)-Ce-Bi bond angles—namely, α and β , marked in Fig. 1(a). Interestingly, as applied external pressure increases on $\text{Ce}_3\text{Pd}_3\text{Bi}_4$, and although the length of each bond in $\text{Ce}_3\text{Pd}_3\text{Bi}_4$ gradually decreases, the bond angle of Pd-Ce-Bi under pressure gradually approaches the bond angle of Pt-Ce-Bi in $\text{Ce}_3\text{Pt}_3\text{Bi}_4$ under ambient pressure. This phenomenon is similar to some strongly correlated materials, and in these systems the bond angles have an important influence on hybridization [33]. From the tendency of bond angles, we deduce that as the pressure increases, the ground

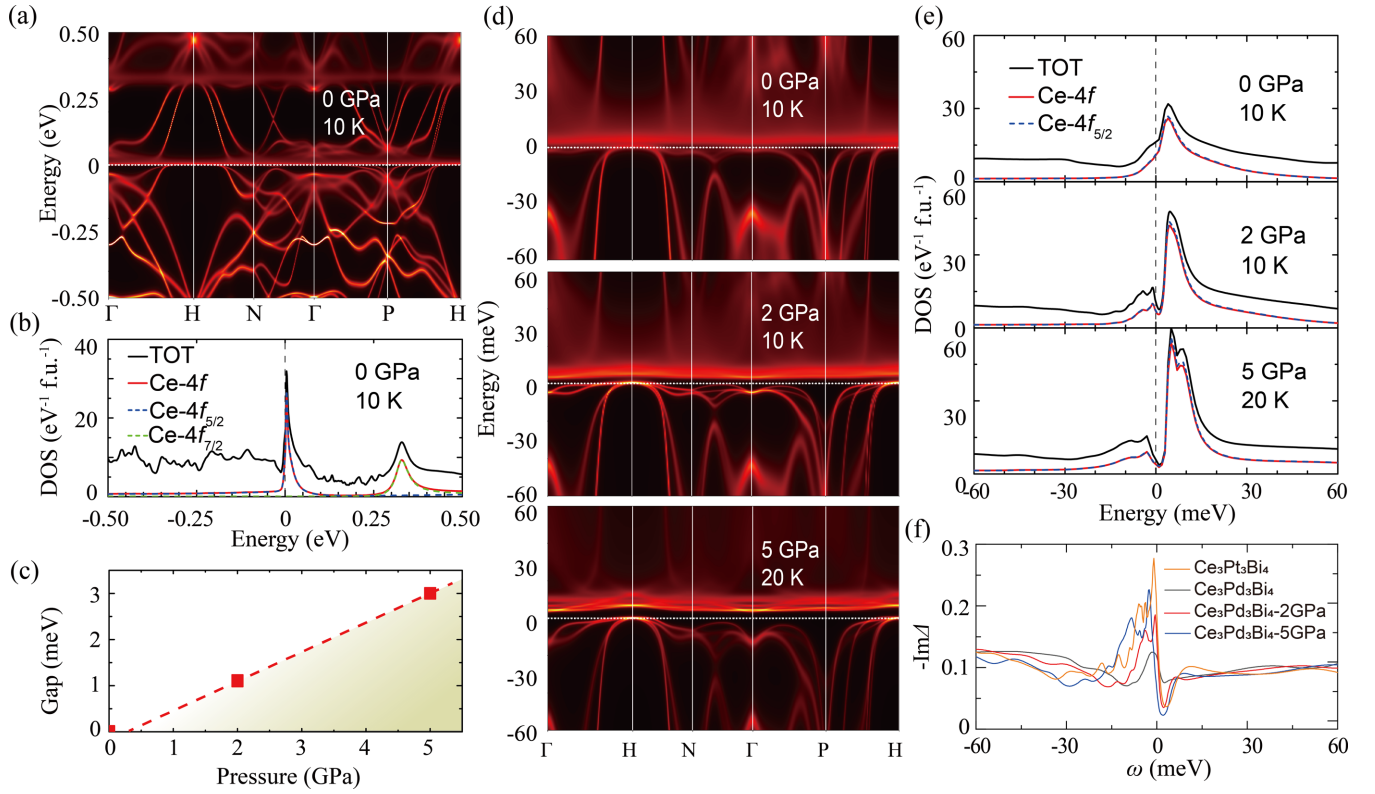


FIG. 3. The electronic structure of $\text{Ce}_3\text{Pd}_3\text{Bi}_4$ under different pressure from DFT + DMFT. The momentum-resolved spectral functions (a) and spectral density (b) of $\text{Ce}_3\text{Pd}_3\text{Bi}_4$ under 0 GPa at 10 K. (c) The gap of $\text{Ce}_3\text{Pd}_3\text{Bi}_4$ under different pressure. The spectral functions (d) and spectral density (e) at different pressures and different temperatures. The black solid lines, red solid lines, blue dashed lines, and green dashed lines represent total spectral density, Ce-4*f*, Ce-4*f*_{5/2}, and Ce-4*f*_{7/2} contributions, respectively. (f) Imaginary part of the impurity hybridization function $\Delta_{5/2}(\omega)$ of $\text{Ce}_3\text{Pt}_3\text{Bi}_4$ under ambient pressure and $\text{Ce}_3\text{Pd}_3\text{Bi}_4$ under different pressure, at 10K.

states of $\text{Ce}_3\text{Pd}_3\text{Bi}_4$ may approach $\text{Ce}_3\text{Pt}_3\text{Bi}_4$, under ambient pressure.

Figures 3(d) and 3(e) gives the electronic structures of $\text{Ce}_3\text{Pd}_3\text{Bi}_4$ under pressure at different temperatures. Compared with the ambient pressure, a small hybridization gap (~ 1.1 meV) begins to appear under 2 GPa, when the temperature drops to 10 K. The formation of the hybridization gap reflects the increasing strength of hybridization. As the pressure increases to 5 GPa, the strength of hybridization

increases significantly. When the temperature is reduced to 20 K, a clear hybridization energy gap appears, and the size (~ 3.0 meV) is close to that of $\text{Ce}_3\text{Pt}_3\text{Bi}_4$. The spectral functions of them are basically similar. Figure 3(c) shows the gaps of $\text{Ce}_3\text{Pd}_3\text{Bi}_4$ under three pressures (ambient pressure, 2 GPa, 5 GPa). The intersection of the connection line between 5 GPa and 2 GPa and the pressure axis is near 0 GPa. Therefore, $\text{Ce}_3\text{Pd}_3\text{Bi}_4$ is at the edge of forming coherent hybridization under ambient pressure. In Fig. 3(f), we

TABLE I. The crystal structure information of $\text{Ce}_3\text{Pt}_3\text{Bi}_4$ and $\text{Ce}_3\text{Pd}_3\text{Bi}_4$ at different pressures. The space group is $I\bar{4}3d$ (No. 220), and the atomic sites are as follows: Ce 12*b* (0.75, 0.625, 0), Pt(Pd) 12*a* (0.75, 0.125, 0), and Bi 16*c* (*x*, *x*, *x*). There are two different Pt(Pd)-Ce-Bi bond angles—namely, α and β , marked in Fig. 1(a).

		$\text{Ce}_3\text{Pt}_3\text{Bi}_4$	$\text{Ce}_3\text{Pd}_3\text{Bi}_4$ (0 GPa)	$\text{Ce}_3\text{Pd}_3\text{Bi}_4$ (2 GPa)	$\text{Ce}_3\text{Pd}_3\text{Bi}_4$ (5 GPa)
<i>a</i> , <i>b</i> , <i>c</i> (Å)	DFT	10.0738	10.0536	9.9784	9.8785
	DFT + <i>U</i>	10.0554	10.0155	9.9410	9.8476
	Exp.	10.051 [11]	10.052 [34]		
Bi (<i>x</i>)		0.9122	0.9139	0.9131	0.9120
Ce-Bi (Å)		3.4381	3.4496	3.4151	3.3702
		3.5362	3.5102	3.4928	3.4690
Pt(Pd)-Bi (Å)		2.8370	2.8230	2.8058	2.7826
Pt(Pd)-Ce-Bi (°)	α	51.213	50.858	51.026	51.239
	β	50.178	50.218	50.198	50.175

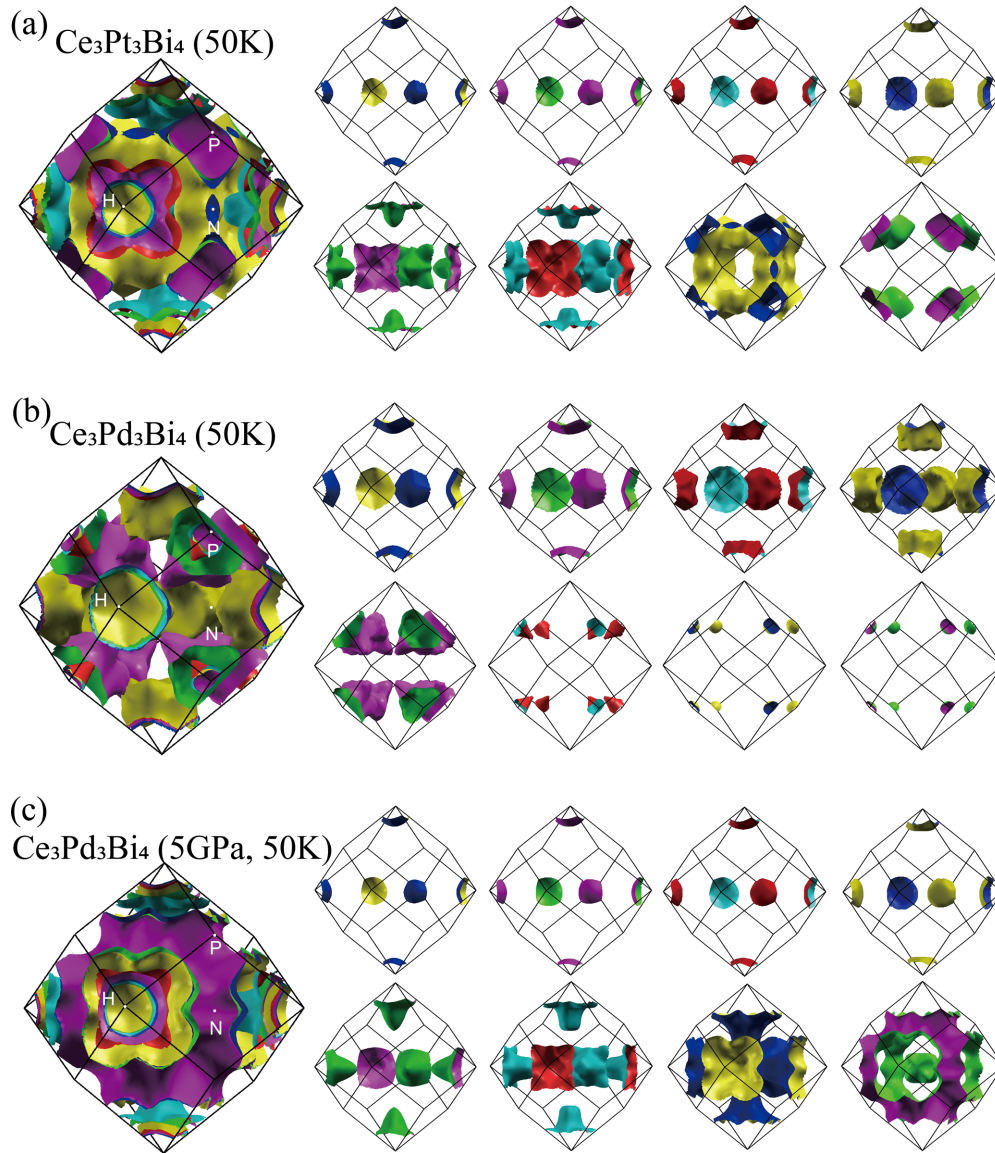


FIG. 4. Fermi surfaces of $\text{Ce}_3\text{Pt}_3\text{Bi}_4$ (a) under ambient pressure and $\text{Ce}_3\text{Pd}_3\text{Bi}_4$ under ambient pressure (b) and 5 GPa (c) at 50 K from DFT + DMFT. The top row in each view is the first four Fermi surfaces; the bottom row in each view is the last four.

show the imaginary part of the hybrid function $-\text{Im}\Delta(\omega)$ near the E_F at 10 K. Under ambient pressure, the peak of $-\text{Im}\Delta(\omega)$ of $\text{Ce}_3\text{Pt}_3\text{Bi}_4$ near the E_F is much larger than that of $\text{Ce}_3\text{Pd}_3\text{Bi}_4$. As the pressure increases, the peak of $-\text{Im}\Delta(\omega)$ of $\text{Ce}_3\text{Pd}_3\text{Bi}_4$ increases gradually. When the pressure is increased to 5 GPa, the height of the peak is close to that of $\text{Ce}_3\text{Pt}_3\text{Bi}_4$ under ambient pressure. This indicates that the hybridization strength of $\text{Ce}_3\text{Pd}_3\text{Bi}_4$ is much lower than that of $\text{Ce}_3\text{Pt}_3\text{Bi}_4$ at ambient pressure. In addition, the pressure will increase the strength of hybridization in $\text{Ce}_3\text{Pd}_3\text{Bi}_4$. When the pressure is increased to 5 GPa, the strength of hybridization is close to that of $\text{Ce}_3\text{Pt}_3\text{Bi}_4$ under ambient pressure. The conduction band components near the E_F are mainly Pt-5d/Pd-4d and Bi-6p. In addition, the lattice constants of the two materials are close at ambient pressure, and as the lattice constant of $\text{Ce}_3\text{Pd}_3\text{Bi}_4$ decreases, the strength of hybridization of $\text{Ce}_3\text{Pd}_3\text{Bi}_4$ gradually nears that of $\text{Ce}_3\text{Pt}_3\text{Bi}_4$. Therefore, we believe that the difference in the strength of

hybridization is due to the different radii of 4d and 5d orbitals.

To give a better understand of electronic structures, Fig. 4 shows the quasiparticle Fermi surfaces of $\text{Ce}_3\text{Pt}_3\text{Bi}_4$ [ambient pressure, Fig. 4(a)] and $\text{Ce}_3\text{Pd}_3\text{Bi}_4$ [ambient pressure, Fig. 4(b), and 5 GPa, Fig. 4(c)] at 50 K by setting the $\text{Im}\Sigma(\omega) = 0$. At 50 K, all three cases are metallic, with eight bands across the E_F . As the pressure of $\text{Ce}_3\text{Pd}_3\text{Bi}_4$ increases, the Fermi surface sheets formed by the lowest four bands at the H point gradually decreases, and the Fermi surface sheets formed by the fifth and sixth bands gradually move from the P point to the H point, whereas the Fermi surface sheets formed by the highest two bands at the P point gradually increase and the eighth bands form the Fermi surface sheets at the Γ point, as show in Figs. 4(b) and 4(c). Pressure causes $\text{Ce}_3\text{Pd}_3\text{Bi}_4$ in the metallic state to produce a Lifshitz transition. As the pressure increases to 5 GPa, the Fermi surface of $\text{Ce}_3\text{Pd}_3\text{Bi}_4$ is similar to that of $\text{Ce}_3\text{Pt}_3\text{Bi}_4$ under ambient pressure, and even

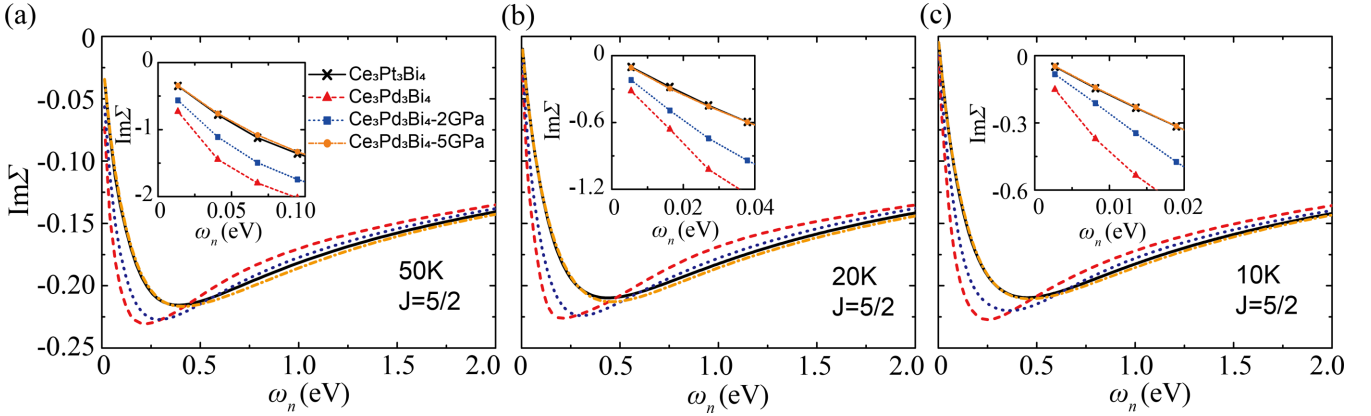


FIG. 5. Imaginary part of self-energy $\Sigma_{5/2}(i\omega_n)$ in Matsubara frequency of $\text{Ce}_3\text{Pt}_3\text{Bi}_4$ under ambient pressure (black solid lines) and $\text{Ce}_3\text{Pd}_3\text{Bi}_4$ under ambient pressure (red dashed lines), 2 GPa (blue dotted lines), and 5 GPa (orange dotted/dashed lines) at 50 K (a), 20 K (b), and 10 K (c).

the seventh and eighth Fermi surface sheets are larger than $\text{Ce}_3\text{Pt}_3\text{Bi}_4$, indicating that their strengths of hybridization are similar.

In order to see the detailed influence of strongly correlated effects, we calculated the imaginary part of self-energy in Matsubara frequency $\text{Im}\Sigma(i\omega_n)$ of $\text{Ce-}4f_{5/2}$ for $\text{Ce}_3\text{Pt}_3\text{Bi}_4$ under ambient pressure and $\text{Ce}_3\text{Pd}_3\text{Bi}_4$ under different pressures (see in Fig. 5). For $\text{Ce}_3\text{Pt}_3\text{Bi}_4$, the $\text{Im}\Sigma_{5/2}(i\omega_n)$ extrapolates to 0 when $\omega_n \rightarrow 0$ at 20 K and 10 K, while it extrapolates to a finite value when $\omega_n \rightarrow 0$ at 50 K, indicating that the system is in the Fermi liquid state at 10 K and 20 K. However, for $\text{Ce}_3\text{Pd}_3\text{Bi}_4$ under ambient pressure, the $\text{Im}\Sigma_{5/2}(i\omega_n)$ extrapolates to a finite value when $\omega_n \rightarrow 0$, even if the temperature is drops to 10 K. As the pressure is increased to 2 GPa, the $\text{Im}\Sigma_{5/2}(i\omega_n)$ extrapolates to 0 when $\omega_n \rightarrow 0$ at 10 K. When the pressure is increased to 5 GPa, the self-energy of $\text{Ce}_3\text{Pd}_3\text{Bi}_4$ is very similar to that of $\text{Ce}_3\text{Pt}_3\text{Bi}_4$ under ambient pressure. This indicates that, as the pressure increases, $\text{Ce}_3\text{Pd}_3\text{Bi}_4$ gradually becomes more coherent.

The self-energy in real-frequency axis $\Sigma(\omega)$ is obtained by the analytical extension of the self-energy in Matsubara frequency $\Sigma(i\omega_n)$ using the maximum entropy method [35,36]. In addition, we also calculated the renormalization factor Z of $\text{Ce-}4f_{5/2}$ from $\Sigma(\omega)$ using $Z^{-1} = 1 - \frac{\partial \text{Re}\Sigma(\omega)}{\partial \omega} \Big|_{\omega=0}$ at 10 K. The results are shown in Table II. Under ambient pressure, Pd-4d is more localized than Pt-5d, hence $\text{Ce}_3\text{Pd}_3\text{Bi}_4$ has a smaller renormalization factor Z of $\text{Ce-}4f_{5/2}$ than $\text{Ce}_3\text{Pt}_3\text{Bi}_4$. However, the small radius of Pd-4d also reduces the strength of hybridization and finally exhibits a metallic ground state without a hybridization gap. As the pressure increases, the atoms in $\text{Ce}_3\text{Pd}_3\text{Bi}_4$ get closer, which leads to the smaller correlation effects and the increase of renormalization factor. When the pressure is increased to 5 GPa, the renormalization factor of $\text{Ce}_3\text{Pd}_3\text{Bi}_4$

TABLE II. Renormalization factor Z of $\text{Ce-}4f_{5/2}$ in $\text{Ce}_3\text{Pd}_3\text{Bi}_4$ under different pressures and $\text{Ce}_3\text{Pt}_3\text{Bi}_4$ at 10 K.

	$\text{Ce}_3\text{Pt}_3\text{Bi}_4$	$\text{Ce}_3\text{Pd}_3\text{Bi}_4$	$\text{Ce}_3\text{Pd}_3\text{Bi}_4$ (2 GPa)	$\text{Ce}_3\text{Pd}_3\text{Bi}_4$ (5 GPa)
Z	0.0476	0.0233	0.0312	0.0466

is very close to that of $\text{Ce}_3\text{Pt}_3\text{Bi}_4$ under ambient pressure. Although pressure reduces the correlation effect, the hybridization between Ce-4f with Pd-4d increases, causing the results to show that pressure drives the metal–insulator transition of $\text{Ce}_3\text{Pd}_3\text{Bi}_4$.

Figure 6 shows the $\text{Im}\Sigma(\omega)$ of $\text{Ce-}4f_{5/2}$ for $\text{Ce}_3\text{Pt}_3\text{Bi}_4$ and $\text{Ce}_3\text{Pd}_3\text{Bi}_4$ at the three lowest temperatures, and the fitted curve using a quadratic function. For metal systems, the range of fitting is $[-T, T]$, and for insulators, it includes the band gap, which is $[-1 \text{ meV}, 5 \text{ meV}]$. For $\text{Ce}_3\text{Pt}_3\text{Bi}_4$, as shown in Fig. 6(a), the $\text{Im}\Sigma_{5/2}(\omega)$ can be well fitted using a quadratic function $\alpha(\omega - \omega_0)^2 + \Sigma_0$ at 10 K and 20 K. The ω_0 is within or near the range of fitting, and Σ_0 is comparable or smaller than the size of gap. However, the ω_0 is far away from the range of fitting at 50 K. Therefore, the Ce-4f_{5/2}-electrons of $\text{Ce}_3\text{Pt}_3\text{Bi}_4$ are coherent when the temperature is below 20 K. For $\text{Ce}_3\text{Pd}_3\text{Bi}_4$, ω_0 is not in the range of fitting, and Σ_0 is much larger than the energy gap even at 10 K, as shown in Fig. 6(b). As the pressure increases to 2 GPa, the $\text{Im}\Sigma_{5/2}(\omega)$ can be well fitted using a quadratic function at 10 K, as shown in Fig. 6(c). When the pressure is further increased to 5 GPa, the $\text{Im}\Sigma_{5/2}(\omega)$ can be well fitted at 20 K and 10 K, and the fitted quadratic function has similar parameters to that of $\text{Ce}_3\text{Pt}_3\text{Bi}_4$ under ambient pressure, as shown in Fig. 6(d). This suggests that applying pressure results in a change in the strength of hybridization of $\text{Ce}_3\text{Pd}_3\text{Bi}_4$, which affects the ground state. Therefore, the conclusion obtained from the $\text{Im}\Sigma_{5/2}(\omega)$ is the same as that presented earlier: $\text{Ce}_3\text{Pd}_3\text{Bi}_4$ is at the edge of forming hybridization and the pressure drives the metal–insulator transition of $\text{Ce}_3\text{Pd}_3\text{Bi}_4$ through changing the correlation effect.

IV. CONCLUSION

In conclusion, we have performed systematic DFT + DMFT studies on $\text{Ce}_3\text{Pt}_3\text{Bi}_4$ under ambient pressure and $\text{Ce}_3\text{Pd}_3\text{Bi}_4$ compounds at different pressures. It is found that $\text{Ce}_3\text{Pt}_3\text{Bi}_4$ is a typical Kondo insulator with an indirect gap of 3 meV, and $\text{Ce}_3\text{Pd}_3\text{Bi}_4$ is a correlated metal. As the pressure increases, $\text{Ce}_3\text{Pd}_3\text{Bi}_4$ becomes a Kondo insulator, and the sizes of the energy gap are 1.1 meV at 2GPa and 3.0 meV at 5GPa. $\text{Ce}_3\text{Pd}_3\text{Bi}_4$ is a suitable material at the edge of forming

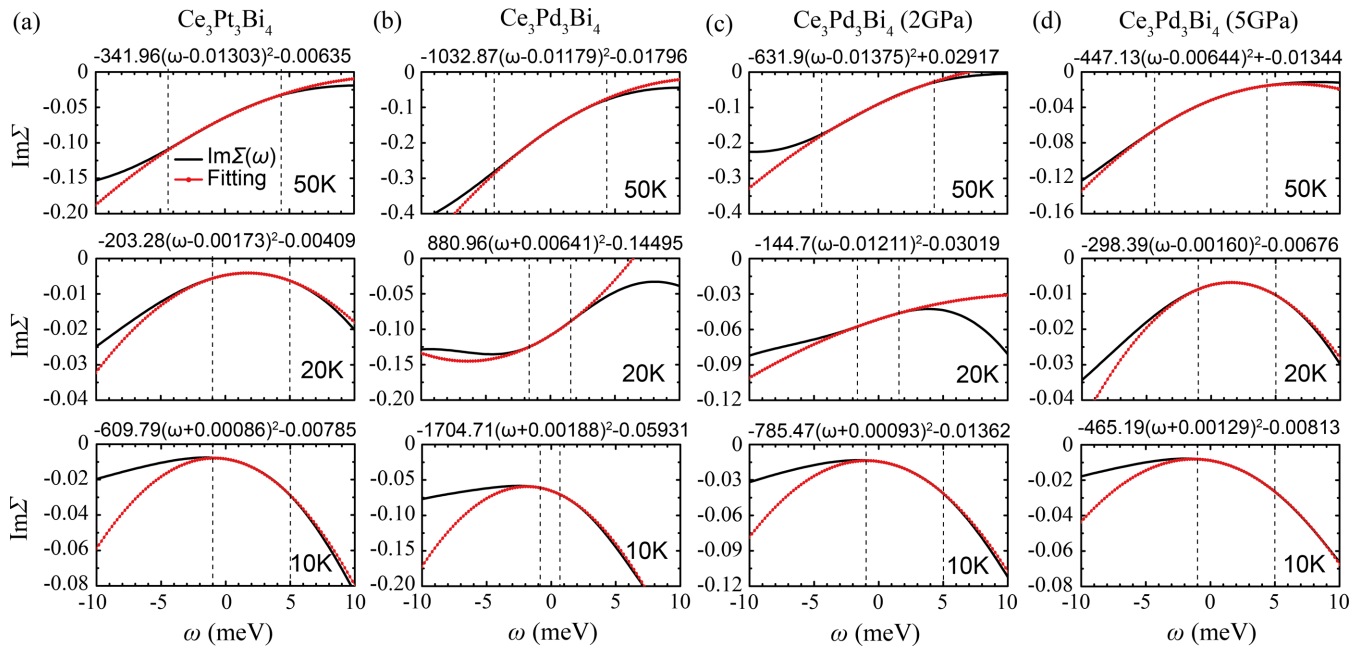


FIG. 6. Imaginary part of self-energy $\Sigma_{5/2}(\omega)$ on real-frequency axis of $\text{Ce}_3\text{Pt}_3\text{Bi}_4$ under ambient pressure (a) and $\text{Ce}_3\text{Pd}_3\text{Bi}_4$ under ambient pressure (b), 2 GPa (c), and 5 GPa (d) at 10, 20, and 50 K. The red dotted line is the quadratic function obtained by fitting.

hybridization, hence the pressure can easily tune the gap by adjusting the strength of hybridization. Our work clarifies the reason for the difference between the two compounds is not that platinum has a stronger SOC than palladium, but that $\text{Ce}_3\text{Pt}_3\text{Bi}_4$ has stronger hybridization due to a larger radius of Pt-5d orbitals.

ACKNOWLEDGMENT

This work was supported by the National Natural Science Foundation of China (Grants No. 12074274 and No. 12204033).

- [1] T. Yoshida, R. Peters, and N. Kawakami, *Phys. Rev. B* **98**, 035141 (2018).
- [2] X.-L. Qi and S.-C. Zhang, *Rev. Mod. Phys.* **83**, 1057 (2011).
- [3] M. Z. Hasan and C. L. Kane, *Rev. Mod. Phys.* **82**, 3045 (2010).
- [4] C. Y. Guo, F. Wu, Z. Z. Wu, M. Smidman, C. Cao, A. Bostwick, C. Jozwiak, E. Rotenberg, Y. Liu, F. Steglich, and H. Q. Yuan, *Nat. Commun.* **9**, 4622 (2018).
- [5] C. Cao, G.-X. Zhi, and J.-X. Zhu, *Phys. Rev. Lett.* **124**, 166403 (2020).
- [6] H.-H. Lai, S. E. Grefe, S. Paschen, and Q. Si, *Proc. Natl. Acad. Sci. USA* **115**, 93 (2018).
- [7] C. Guo, C. Cao, M. Smidman, F. Wu, Y. Zhang, F. Steglich, F.-C. Zhang, and H. Yuan, *npj Quantum Mater.* **2**, 39 (2017).
- [8] S. Dzsaber, L. Prochaska, A. Sidorenko, G. Eguchi, R. Svagera, M. Waas, A. Prokofiev, Q. Si, and S. Paschen, *Phys. Rev. Lett.* **118**, 246601 (2017).
- [9] P.-Y. Chang and P. Coleman, *Phys. Rev. B* **97**, 155134 (2018).
- [10] S. K. Kushwaha, M. K. Chan, J. Park, S. M. Thomas, E. D. Bauer, J. D. Thompson, F. Ronning, P. F. S. Rosa, and N. Harrison, *Nat. Commun.* **10**, 5487 (2019).
- [11] K. Takegahara, H. Harima, Y. Kaneta, and A. Yanase, *J. Phys. Soc. Japan* **62**, 2103 (1993).
- [12] Y. Takeda, M. Arita, H. Sato, K. Shimada, H. Namatame, M. Taniguchi, K. Katoh, F. Iga, and T. Takabatake, *J. Electron. Spectrosc. Relat. Phenomena* **101–103**, 721 (1999).
- [13] M. F. Hundley, J. D. Thompson, P. C. Canfield, and Z. Fisk, *Physica B* **199–200**, 443 (1994).
- [14] M. F. Hundley, P. C. Canfield, J. D. Thompson, Z. Fisk, and J. M. Lawrence, *Physica B* **171**, 254 (1991).
- [15] M. O. Ajeesh, S. M. Thomas, S. K. Kushwaha, E. D. Bauer, F. Ronning, J. D. Thompson, N. Harrison, and P. F. S. Rosa, *Phys. Rev. B* **106**, L161105 (2022).
- [16] C. Xu, C. Cao, and J.-X. Zhu, *npj Quantum Mater.* **7**, 18 (2022).
- [17] P. Blaha, K. Schwarz, G. K. Madsen, D. Kvasnicka, and J. Luitz, *WIEN2K: An Augmented Plane Wave + Local Orbitals Program for Calculating Crystal Properties* (Karlheinz Schwarz, Techn. Universitat Wien, Austria, 2001).
- [18] J. P. Perdew, K. Burke, and M. Ernzerhof, *Phys. Rev. Lett.* **77**, 3865 (1996).
- [19] G. Kotliar, S. Y. Savrasov, K. Haule, V. S. Oudovenko, O. Parcollet, and C. A. Marianetti, *Rev. Mod. Phys.* **78**, 865 (2006).
- [20] K. Haule, *Phys. Rev. B* **75**, 155113 (2007).
- [21] J. H. Shim, K. Haule, and G. Kotliar, *Science* **318**, 1615 (2007).
- [22] K. Haule, J. H. Shim, and G. Kotliar, *Phys. Rev. Lett.* **100**, 226402 (2008).
- [23] K. Haule, C.-H. Yee, and K. Kim, *Phys. Rev. B* **81**, 195107 (2010).
- [24] Y.-C. Wang, Y.-J. Xu, Y. Liu, X.-J. Han, X.-G. Zhu, Y.-f. Yang, Y. Bi, H.-F. Liu, and H.-F. Song, *Phys. Rev. B* **103**, 165140 (2021).

- [25] V. Vildosola, A. M. Llois, and J. G. Sereni, *Phys. Rev. B* **69**, 125116 (2004).
- [26] V. Vildosola, A. M. Llois, and M. Alouani, *Phys. Rev. B* **71**, 184420 (2005).
- [27] N. Wakeham, P. F. S. Rosa, Y. Q. Wang, M. Kang, Z. Fisk, F. Ronning, and J. D. Thompson, *Phys. Rev. B* **94**, 035127 (2016).
- [28] A. Severing, J. D. Thompson, P. C. Canfield, Z. Fisk, and P. Riseborough, *Phys. Rev. B* **44**, 6832 (1991).
- [29] J. C. Cooley, M. C. Aronson, and P. C. Canfield, *Phys. Rev. B* **55**, 7533 (1997).
- [30] B. Bucher, Z. Schlesinger, P. C. Canfield, and Z. Fisk, *Phys. Rev. Lett.* **72**, 522 (1994).
- [31] K. Harun, N. A. Salleh, B. Deghfel, M. K. Yaakob, and A. A. Mohamad, *Results Phys.* **16**, 102829 (2020).
- [32] M. E. Arroyo-de Dompablo, A. Morales-García, and M. Taravillo, *J. Chem. Phys.* **135**, 054503 (2011).
- [33] C. Petrovic, Y. Lee, T. Vogt, N. D. Lazarov, S. L. Bud'ko, and P. C. Canfield, *Phys. Rev. B* **72**, 045103 (2005).
- [34] W. Hermes, S. Linsinger, R. Mishra, and R. Pöttgen, *Monatsh. Chem.* **139**, 1143 (2008).
- [35] R. N. Silver, D. S. Sivia, and J. E. Gubernatis, *Phys. Rev. B* **41**, 2380 (1990).
- [36] M. Jarrell and J. E. Gubernatis, *Phys. Rep.* **269**, 133 (1996).